Graphene-based optical phase modulation of waveguide transverse electric modes

Michele Midrio,[1] Paola Galli,[2] Marco Romagnoli,[3,*] Lionel C. Kimerling,[4] and Jurgen Michel[4]

[1]*Dipartimento di Ingegneria Elettrica Gestionale e Meccanica, Università degli Studi di Udine, 33100 Udine, Italy*
[2]*Bell Labs, Alcatel-Lucent, via Trento 30, 20871 Vimercate (MB), Italy*
[3]*CNIT National Laboratory of Photonic Networks, 56124 Pisa, Italy*
[4]*Massachusetts Institute of Technology, 77 Massachusetts Ave., Cambridge, Massachusetts 02139, USA*
**Corresponding author: marco.romagnoli@cnit.it*

Received January 17, 2014; revised March 25, 2014; accepted March 27, 2014;
posted April 3, 2014 (Doc. ID 204777); published May 9, 2014

In this paper we report TE-mode phase modulation obtained by inducing a capacitive charge on graphene layers embedded in the core of a waveguide. There is a biasing regime in which graphene absorption is negligible but large index variations can be achieved with a voltage–length product as small as $V_\pi L_\pi \simeq 0.07$ V cm for straight waveguides and $V_\pi L_\pi \simeq 0.0024$ V cm for 12 μm radius microring resonators. This phase modulation device uniquely enables a small signal amplitude <1 V with a micrometer-sized footprint for compatibility with CMOS circuit integration. Examples of phase-induced changes are computed for straight waveguides and for microring resonators, showing the possibility of implementing several optoelectronic functionalities as modulators, tunable filters, and switches.

OCIS codes: (060.4510) Optical communications; (130.3130) Integrated optics materials; (250.3140) Integrated optoelectronic circuits; (130.4110) Modulators.
http://dx.doi.org/10.1364/PRJ.2.000A34

1. INTRODUCTION

Fundamental properties and potential applications of carbon-based structures are of interest in emerging nanoelectronics and nanophotonics. Graphene is a planar atomic layer of carbon atoms bonded in a hexagonal structure that has shown fundamental physical properties different from those of semiconductors [1]. In graphene, the energy-momentum dispersion is linear over a wide range of energies in contrast to the typical parabolic shape of semiconductor valence and conduction bands. This linearity leads to a zero gap and to a massless condition for electrons, with a consequent energy-independent velocity analogous to sound waves. Another property of graphene is the single layer, or 2D, structure that leads to an enhancement of the interface electric field that may be used for controlling large carrier concentrations with low gating voltages. Integrated optical modulators in silicon are key components in a photonic circuit. The basic mechanisms that alter the amplitude or phase of the propagating light are based on different effects. The plasma dispersion effect is the most used; in this case electrically induced change in the carrier concentration provides a change in material absorption and refractive index proportional to the carrier density [2]. However, due to the nature of the physical mechanism, phase and amplitude variation never act independently. In addition, residual carrier density occurring under modulation or partial field overlap with electrodes limits performance in extinction ratio or in insertion loss. The Franz–Keldysh effect and the quantum confined Stark effect (QCSE) are alternative mechanisms used in Ge p-i-n or in Ge and III-V quantum wells [3,4]. In these cases the effect is limited to the spectral band near the semiconductor band edge. As for plasma-dispersion-based devices, even in this case insertion loss due to carriers must be traded off at the expense of a large extinction ratio. Recently a single sheet of graphene on a silicon waveguide has been reported to provide efficient, low-consumption electroabsorption modulation [5]. In the reported modulator the interband transitions of photogenerated electrons are modulated over broad spectral ranges by the drive voltage, so an efficient broadband optical graphene modulator has been demonstrated.

By changing the graphene modulator biasing, is possible to discriminate amplitude against phase modulation. This property, theoretically predicted by Xu *et al.* [6], is specific of graphene and indicates that beyond the conventional absorption modulation graphene can be used as a phase modulator with a negligible contribution in amplitude modulation. The wavelength independence of graphene, along with the unique property of bias-induced separation of electroabsorption and electro-refractive modulation, makes this material suitable for a highly efficient modulator for complex modulation formats (combination of phase and amplitude modulation). These previous studies on graphene-based phase modulation were carried out for TM modes in different waveguide geometries [6,7]. In particular, in Ref. [7] a modulation voltage–length product of $V_\pi L_\pi \simeq 0.04$ V cm has been demonstrated. This result should be compared with the result of the SISCAP modulator [8] that exploits an analogous waveguide structure. The SISCAP modulator is based on charge accumulation on a thin insulating dielectric placed in the middle of the waveguide section. For the SISCAP modulator, $V_\pi L_\pi \simeq 0.2$ V cm. In standard charge-depletion Si modulators, the product instead is $V_\pi L_\pi \simeq 2$ V cm [9]. In this paper we will consider a practical design of a graphene-based phase modulator based on the TE mode. This because in a practical

photonic circuit including other components, polarization is TE. In this work we show that the modulator voltage–length product is $V_\pi L_\pi \simeq 0.07$ V cm in a straight waveguide and is $V_\pi L_\pi \simeq 0.0024$ V cm in a 12 μm radius microring structure. We highlight the unique advantage of using graphene together with deposited dielectrics. In fact, we report on a practical structure based on alternate SiN and graphene deposition that makes this modulator suitable for a very wide range of wavelengths spanning from IR to visible. In addition we chose SiN to demonstrate modulation in a material that normally is only passive. This is important because, thanks to graphene, we could consider materials other than conventional silicon or germanium for the design of photonic integrated circuits. For instance, graphene applied to polymers allows modulation in plastic waveguides.

We report on an evaluation of the energy consumption in the TE-type graphene modulator. In addition we emphasize that because the phase variation is based on a capacitor charge, this device can also be used for trimming and switching applications. The advantage is twofold: phase-only change and no current injection. This permits us to control all interferometric structures in a complex photonic integrated circuit (filters and switches) with no extra loss and no power consumption.

2. PRINCIPLE OF OPERATION

One of the many remarkable and unique properties of graphene is that its complex conductivity can be tuned, even at optical frequencies, by varying the applied chemical potential, i.e., by adding or removing charges from the graphene sheet. The dependence of the complex graphene's conductivity (σ) on frequency (ω), temperature (T), and applied chemical potential (μ_C) has been discussed in several papers (see, for instance, [10–13]). It turns out that

$$\sigma_{\mathrm{R}} \simeq \frac{\sigma_0}{2}\left(\tanh\frac{\hbar\omega + 2\mu_C}{4k_BT} + \tanh\frac{\hbar\omega - 2\mu_C}{4k_BT}\right), \tag{1}$$

$$\sigma_{\mathrm{I}} \simeq \sigma_0\left[\frac{4|\mu_c|}{\pi\omega} - \frac{1}{2\pi}\log\frac{(\omega + |2\mu_C|)^2}{(\omega - 2|\mu_C|)^2 + (2T)^2}\right], \tag{2}$$

where $\hbar$ and k_B are the reduced Planck's and Boltzmann constants, respectively, and

$$\sigma_0 = \frac{e^2}{4\hbar} \simeq 6.0853 \times 10^{-5}\ \text{Siemens}, \tag{3}$$

with e as the electron charge. The relative dielectric constant of graphene is simply related to the imaginary part of its conductivity as follows:

$$\epsilon_r = 1 + \frac{\sigma_{\mathrm{I}}}{\omega\epsilon_0}, \tag{4}$$

with $\epsilon_0 = 8.85 \times 10^{-12}$ F/m.

A plot of Eqs. (1)–(4) is reported in Fig. 1 for $\hbar\omega = 0.8$ eV (corresponding to a free-space wavelength of 1550 nm) in the range of chemical potentials that will be used in the present paper. The upper panel is related to the absorption coefficient of graphene. The lower panel refers to the dielectric constant.

In the present paper we show that if properly biased, a variation of the imaginary part of graphene's conductivity may produce a visible change of the *phase* of the propagating wave. Notice that Eqs. (1) and (4) show that when a bias is applied to a graphene layer, both the real and imaginary parts of its conductivity change. Thus, a modulator based on the tunability of graphene's complex conductivity will in general modulate both the phase and the amplitude of the optical wave.

In order to separate amplitude or phase modulation, different operating ranges must be used. With reference to Fig. 1, for $|\mu_C|$ between 0.3 and 0.5 eV, a large variation of the real part of graphene's conductivity is observed (see the inset in the upper panel of the figure). In the same range, the imaginary part of the conductivity changes as well [see Eqs. (1) and (4)], leading to a signal that is modulated in both amplitude and phase.

In the range $|\mu_C| > 0.5$ eV, the real part of graphene conductivity drops to negligible values: graphene has become an optically transparent material. Any change of the conductivity will now reflect on the dielectric constant only, eventually leading to phase modulation of the traveling signal.

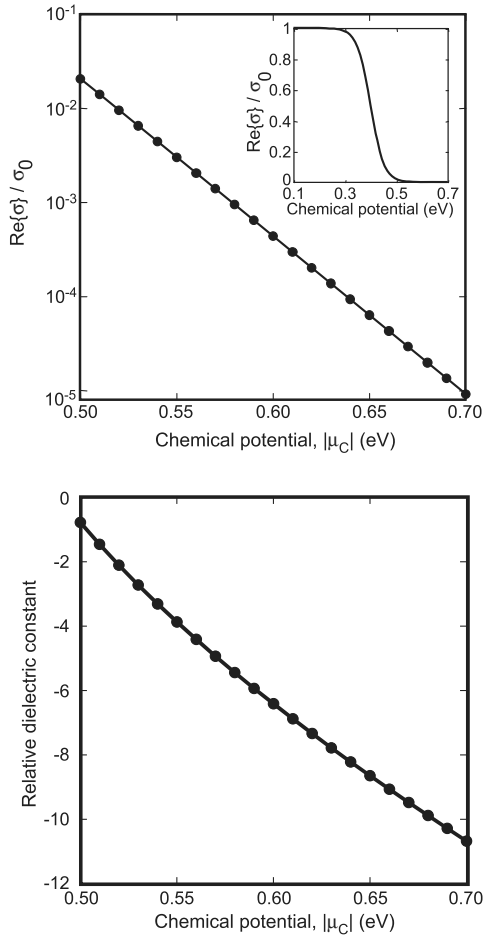

Fig. 1. Upper panel: real part of the graphene conductivity for $\hbar\omega = 0.8$ eV (corresponding to a free-space wavelength equal to 1550 nm) versus the applied chemical potential μ_C. Inset: same quantity on a broader range of applied chemical potentials. Lower panel: relative dielectric constant of graphene versus the applied chemical potential.

3. PHASE MODULATION IN THE STRAIGHT-WAVEGUIDE CONFIGURATION

Graphene's conductivity can be changed by adding (or removing) electrical charges to it. As shown by Liu in Ref. [14], an efficient way to obtain this is to realize a capacitor in which both plates are formed by graphene layers entering into the waveguide core. A schematic diagram of such a waveguide is depicted in Fig. 2.

The relationship among the carrier density n_S on the graphene sheets, the chemical potential μ_C, and the applied voltage V is the following:

$$n_s = \frac{2}{\pi\hbar^2 v_F^2}\int_0^{+\infty} \epsilon[f_d(\epsilon) - f_d(\epsilon + 2\mu_C)]\mathrm{d}\epsilon \simeq \frac{\mu_C^2}{\pi\hbar^2 v_F^2}, \quad (5)$$

where $f_d(\epsilon) = (e^{(\epsilon-\mu_C)/k_BT)} + 1)^{-1}$ is the Fermi–Dirac distribution, $v_F \simeq 9.5 \times 10^5$ m/s, and

$$V = \frac{d}{\epsilon_0 \epsilon_{\mathrm{Oxide}}} \frac{|e|}{\pi\hbar^2 v_F^2}\mu_C^2 + 2|\mu_C|. \quad (6)$$

Numerical simulations with the waveguide schematically depicted in Fig. 2 were performed. A waveguide comprising two layers of graphene (each having a thickness equal to 0.34 nm) was used. The graphene layers were separated by 7 nm of alumina. Silicon-enriched nitride ($Si_xN_{(1-x)}$) was the dielectric forming the high-index contrast waveguide. The cladding was silica.

The dielectric constants used in simulations were equal to 4.7568 for silicon-enriched nitride and 2.25 for silica. The waveguide height and width were 400 and 900 nm, respectively. Propagation of the fundamental TE mode was considered at the propagating wavelength $\lambda_0 = 1550$ nm.

For values of the chemical potential between 0.50 and 0.70 eV, we varied the real and imaginary parts of the complex graphene's conductivity, and we numerically computed the complex effective index of the fundamental TE mode. Results of this analysis are reported in Fig. 3.

The upper panel of Fig. 3 shows the phase change per unit length that is observed when varying the applied chemical potential. Consider a phase modulator working in the range of chemical potentials spanning 0.50–0.60 eV. A phase shift of $\sim(-30\pi)$ rad would be obtained in this case for each centimeter of waveguide. A full $-\pi$ phase shift would require a waveguide length equal to ~340 μm. Observe, however, that the lower panel of the figure shows that whenever $\mu_C = 0.50$, a non-negligible absorption is still present, due to the residual real part of the graphene's conductivity. This is in the order of 4.8 dB/mm for $\mu_C = 0.50$ eV, dropping to

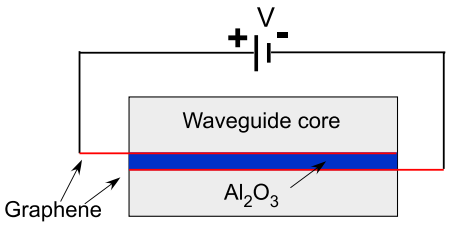

Fig. 2. Schematic diagram (not to scale) of a waveguide comprising two graphene layers (red lines) biased so as to obtain electrochemical doping inside the waveguide core. The blue region is alumina.

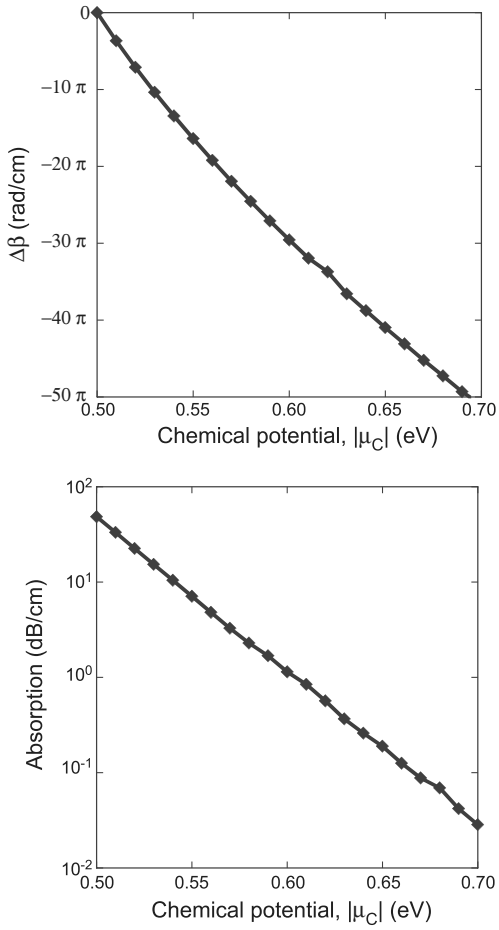

Fig. 3. Upper panel: variation of the phase constant versus the chemical potential. Zero is arbitrarily chosen in correspondence to the phase displacement experienced by the wave when $\mu_C = 0.50$ eV. Lower panel: attenuation across a 1 cm long straight waveguide versus the applied chemical potential. Note the log scale in the vertical axis. Computations have been made for $\lambda = 1550$ nm.

0.1 dB/mm for $\mu_C = 0.60$ eV. The differential absorption across 340 μm of waveguide would hence be in the order of 1.6 dB.

A better result in terms of residual amplitude modulation could be obtained by switching the chemical potential from, say, 0.60–0.70 eV. A phase shift of about (-21π) rad would be obtained in this case for each centimeter of waveguide. A 480 μm long waveguide would hence be needed in order to obtain a full $-\pi$ phase modulation. The residual amplitude modulation, however, would now be limited to less than 0.1 dB.

From Eq. (6) one finds $V = \{3.6, 5.0, 6.5\}$ V for $\mu_C = \{0.5, 0.6, 0.7\}$ eV, respectively, with $\epsilon_{\mathrm{Oxide}} = 10$ (alumina). This way, the electro-optical efficiency is 0.7π/mm/V ($V_\pi L_\pi \simeq 0.07$ V cm) in the range of chemical potentials from 0.6 to 0.7 eV.

The π shift voltage–length product for graphene is much smaller than, for instance, in plasma-dispersion-based silicon modulators where $V_\pi L_\pi \simeq 2$ V cm [9]. Interestingly, this occurs even if the index variation takes place in the present case only in the graphene layer, which is extremely thin. In order to give a quantitative explanation of such a large effect, let us assume that the waveguide mode amplitude is constant within

the core and null outside. By using the variational theorem applied to the variation of the dielectric constant (say $\Delta\epsilon_{\mathrm{rel}}$) of a thin film in a waveguide, one obtains [15]

$$\Delta n_{\mathrm{eff}} = \frac{\Delta\epsilon_r}{2n_{\mathrm{eff}}}\left(\frac{h}{H}\right).$$

In our waveguide, the fundamental TE mode has the effective index $n_{\mathrm{eff}} \simeq 1.735$. Assume that initially, the graphene layers are polarized so that $|\mu_C| = 0.5$ eV. From Eq. (4), one finds that the corresponding relative dielectric constant of the layers is $\epsilon_r \simeq 0.5$. By increasing the chemical potential to 0.6 eV, the relative dielectric constant of the layers becomes $\epsilon_r = -6.2$. The overall change in relative dielectric constant for two graphene layers is $\Delta\epsilon_r = -11.2$, after summing the variations in the two graphene layers as they occurred over a single layer with thickness $h = 0.34$ nm. It then turns out that $\Delta n_{\mathrm{eff}} \simeq -2.8 \times 10^{-3}$. Numerically, we found $\Delta n_{\mathrm{eff}} \simeq -2.3 \times 10^{-3}$ (which corresponds to the phase shift of -30π/cm we mentioned above), in reasonable agreement with the above theoretical prediction if one takes into account the fact that the mode profile is not simply constant over the core and zero outside.

In order to compute power consumption of the modulator, we evaluate the required charge for the capacitor, defined by the area S, the capacitance C, and a value of chemical potential μ_C:

$$Q = n_S|e|S \simeq \frac{\mu_C^2|e|S}{\pi\hbar^2 v_F^2}, \tag{7}$$

using Eq. (5). The capacitor capacitance is $C = S\epsilon_0\epsilon_{\mathrm{Oxide}}/d$, and the energy required for switching in a random bit stream is

$$E = \frac{\Delta Q^2}{4C}. \tag{8}$$

In the case of Fig. 3, for a chemical potential variation $\mu_C = 0.5$ eV to $\mu_C = 0.6$ eV (modulator length L = 340 μm), the capacitor surface and capacitance are $S \simeq 3 \times 10^{-6}$ cm^2 and $C \simeq 3.9$ pF, respectively, with a 7 nm alumina spacer (RF dielectric constant = 10). Moreover, from Eq. (7), the charge on each of the capacitor plates is

$$Q_{0.5} \simeq 9.96 \times 10^{-12}\ \text{Coulomb},$$

$$Q_{0.6} \simeq 1.43 \times 10^{-11}\ \text{Coulomb},$$

for $\mu_C = 0.5$ eV and 0.6 eV, respectively. Therefore, the switching energy is

$$E = \frac{Q_{0.6}^2 - Q_{0.5}^2}{4C} \simeq 7\ \text{pJ}.$$

For a 10 Gbit/s bit rate, this converts into a power consumption $P = 70$ mW, whereas for 25 Gbits/s, $P = 175$ mW or, in general, 7 mW/GHz. This result is analogous to the SISCAP [8]. In fact the geometry is similar; the accumulation occurs on the same dielectric thickness in the center of the capacitor. Currently the SISCAP is the most efficient and compact Si modulator.

4. PHASE MODULATION IN THE RING CONFIGURATION

The straight waveguide configuration has the advantage of being inherently wideband. On the downside, phase modulation in straight waveguides requires rather long propagation. We now aim to show that full phase modulation can be obtained in a much more compact device if a ring configuration is considered instead. Clearly microring resonances imply reduction of bandwidth. However, we show in the following that operations over bands in the order of hundreds of gigahertz can still be obtained, with footprint dimensions limited to hundreds of square micrometers.

In Fig. 4 we show a schematic diagram of the all-pass microring filter we use as an example of the effect of the change of graphene conductivity in the filter phase shift. The filter contains a straight bus waveguide made of silicon-enriched nitride $W_{\mathrm{bus}} = 700$ nm wide and $H_{\mathrm{bus}} = 400$ nm high that is coupled to a microring. The microring waveguide contains two layers of graphene, and its width is $W_{\mathrm{ring}} = 900$ nm. Bus-to-ring gaps where chosen in the range $g \simeq 100/200$ nm, and the microring radius $R_e \simeq 9/15$ μm.

The lower panel of Fig. 4 shows the fields in the ring and in the bus. The input-to-output transfer function reads [16,17]

$$\frac{b_1}{a_1} = \frac{t - \alpha e^{-i\varphi}}{1 - \alpha t e^{-i\varphi}}. \tag{9}$$

We remark that in this equation α is the amplitude transmission of the field through a single ring round trip, while t is the bus-to-bus (or ring-to-ring) coupler transmission, respectively. Moreover, φ is the field phase shift in a single ring round trip. Let us now denote as T and ψ the amplitude and phase transfer function of the ring structure, respectively. They read

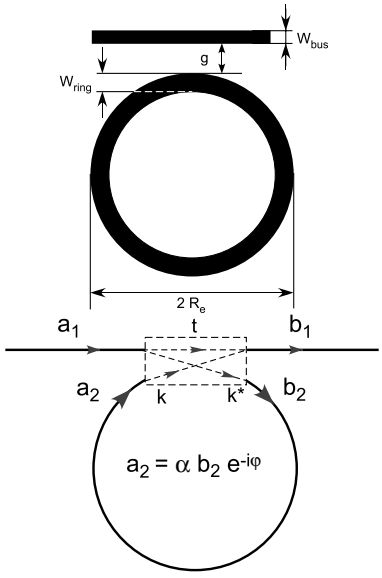

Fig. 4. Upper panel: schematic diagram of the ring configuration phase modulator. Lower panel: fields in the ring structure, with definition of the straight waveguide and ring single-pass transmission, t and α, respectively. The cross section of the waveguide in the ring is the same as in Fig. 2.

$$T = \left|\frac{b_1}{a_1}\right|^2 = \frac{(\alpha - |t|)^2}{(1 - \alpha|t|)^2}, \tag{10}$$

$$\psi = \text{phase}\left(\frac{b_1}{a_1}\right) = \arctan\left(\frac{\alpha(1-t^2)\sin\varphi}{t(1+\alpha^2) - \alpha(1+t^2)\cos\varphi}\right). \tag{11}$$

Plots of Eqs. (10) and (11) are reported in the upper and lower panels of Fig. 5, respectively. Coupler transmission $t = 0.9$ was used (i.e., power coupling coefficient of 18.5%), along with $\alpha = 0.99$ (dashed line) and $\alpha = 0.999$ (solid line). These values would correspond to a ring loss equal to 1.2 dB/mm and 0.1 dB/mm, respectively, when the ring radius is equal to 12 μm. The large coupling in the example is to show the efficiency of the resonant phase shift even for designs highly tolerant to fabrication errors on the centering of the resonant wavelength. Lower values of the coupling coefficient would enhance the graphene-induced phase shift but would be more critical because of the need to trim of the microring resonant frequency.

Dashed and solid lines are also used in the lower panel of Fig. 5, but they almost coincide. If we had further increased the ring transmission $\alpha \to 1$, the amplitude transfer function T would have been flat (i.e., the ring would have behaved as an ideal all-pass filter), while the phase curve would have remained unchanged.

In a real device the combination of a low-loss ring waveguide and low-loss graphene (when biased properly) leads to an almost ideal all-pass filter, i.e., to a device with small insertion loss and large externally induced phase change. This differs from other phase modulation effects achievable in photonic integrated circuits in which phase modulation is always at the expense of a large insertion loss caused by a non-negligible contribution of induced absorption; see, for instance, the plasma dispersion effect, Franz–Keldysh effect, or even the QCSE.

Thus, phase modulation can be achieved by varying only the refractive index of the waveguide in the ring. This leads to filter frequency tuning that can be exploited for tuning/trimming, switching, or modulation. In all these respects, we believe that graphene may offer unique opportunities. As a matter of fact, we have shown above that there is a wide range of chemical potentials that give rise to negligible absorptions: the lower panel of Fig. 3 shows that absorption is lower than 1 dB/cm for chemical potentials above $\mu_C = 0.58$ eV. It would drop even further for $\mu_C > 0.7$ eV, but the breakdown voltage of the dielectric in the capacitor limits too large bias voltages. At the same time, graphene's relative dielectric constant varies by a factor of 2 over the $0.58 < |\mu_C| < 0.70$ eV range.

Figure 6 shows the behavior of the ring as a phase modulator. In the upper panel, the phase shift ψ versus frequency is shown for chemical potential $|\mu_C| = 0.56$ eV (filled diamonds), $|\mu_C| = 0.58$ eV (filled squares), $|\mu_C| = 0.60$ eV (filled circles), $|\mu_C| = 0.62$ eV (empty diamonds), $|\mu_C| = 0.64$ eV

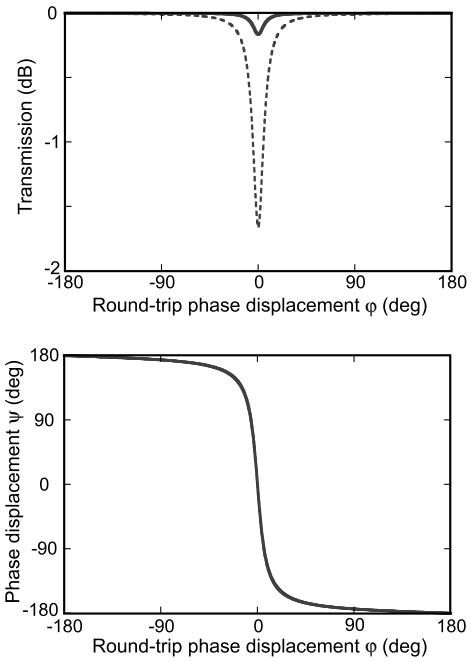

Fig. 5. Upper panel: overall bus-to-bus transmission for coupler transmission $t = 0.9$ and ring transmission $\alpha = 0.99$ (dashed line) or $\alpha = 0.999$ (solid line). The abscissa is the round-trip phase shift φ. Lower panel: overall bus-to-bus phase shift. Dashed and solid lines still refer to $\alpha = 0.99$ and $\alpha = 0.999$ and coincide.

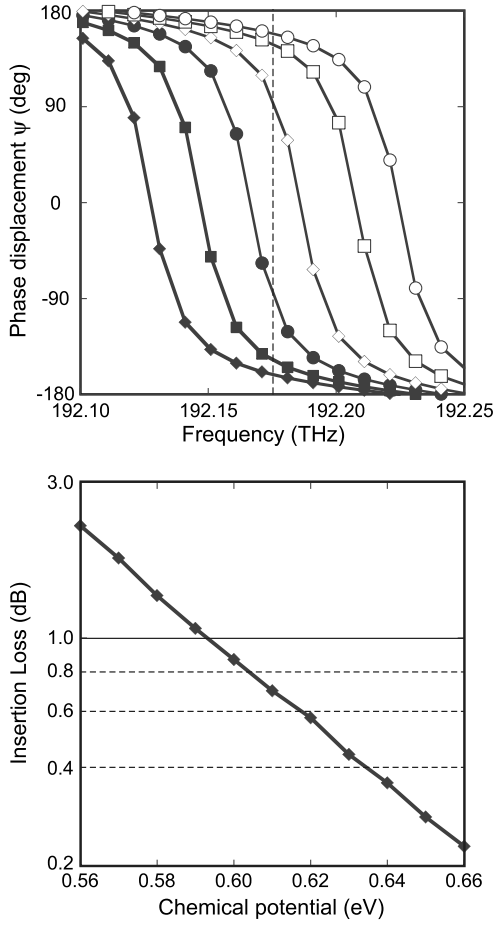

Fig. 6. Upper panel: phase displacement ψ versus frequency for chemical potential $|\mu_C| = 0.56$ eV (filled diamonds), $|\mu_C| = 0.58$ eV (filled squares), $|\mu_C| = 0.60$ eV (filled circles), $|\mu_C| = 0.62$ eV (empty diamonds), $|\mu_C| = 0.64$ eV (empty squares), and $|\mu_C| = 0.66$ eV (empty circles). Lower panel: insertion loss versus the applied chemical potential.

(empty squares), and $|\mu_C| = 0.66$ eV (empty circles). In the lower panel, insertion loss versus the applied chemical potential is shown. A few comments are in order: phase curves are in close agreement with theoretical ones [see Eq. (11) and Fig. 5]. Wide phase modulation can be achieved upon application of a relatively small change in the chemical potential. At any given frequency, a full 180° phase shift requires a variation of the chemical potential in the order of 0.02 eV [corresponding to ≃0.3 V through Eq. (6)]. For instance, the vertical dashed line in the upper panel of Fig. 6 shows the phase shift for a frequency equal to 192.17 THz. The phase is lower than −90° when $\mu_C = 0.60$ eV (filled circles), whereas it is roughly equal to +90° for $\mu_C = 0.62$ eV (empty diamonds).

Insertion losses are lower than 1.0 dB for any chemical potential larger than 0.6 eV. In addition, a change in the chemical potential in the order of 0.02 eV causes a really minor variation of losses. That is, almost pure phase modulation without residual amplitude modulation can be achieved. In terms of both losses and achievable phase shift, the operating point of the device can be anywhere in the range $\mu_C > 0.6$ eV. This suggests that the device could be operated with a bias to set the operation frequency, and full phase shift through modulation of the applied voltage around the bias. This way, trimming of the resonant frequency without heating can be achieved and the complete functionality can be operated with negligible power consumption. Finally, observe that the bandwidth of operation depends solely on the applied voltage to induce the modification of the graphene's dielectric constant. Thanks to the efficiency of the effect, it is not necessary to resort to a large cavity Q to enhance the effect. The choice of the cavity Q would only impact the steepness of the phase transition across the resonant frequency.

The energy consumption for the $R = 12$ μm ring modulator requires a variation of chemical potential μ_C from 0.60 to 0.62 eV, which is less than for the straight phase modulator. In this case, the ring surface and capacitance are $S \simeq 0.67 \times 10^{-6}$ cm^2 and $C \simeq 0.85$ pF, respectively, with an alumina layer equal to 7 nm (RF dielectric constant = 10). From Eq. (7), the charge on the plates for $\mu_C = 0.60$ eV and 0.62 eV are, respectively,

$$Q_{0.60} \simeq 3.18 \times 10^{-12} \text{ Coulomb},$$

$$Q_{0.62} \simeq 3.40 \times 10^{-12} \text{ Coulomb},$$

Therefore, the switching energy is

$$E = \frac{Q_{0.62}^2 - Q_{0.60}^2}{4C} \simeq 0.4 \text{ pJ}$$

For a 10 Gbit/s bit rate, the power consumption is $P = 4$ mW, whereas for 25 Gbits/s, $P = 10$ mW or, in general, 0.4 mW/GHz or 400 fJ/bit. The power consumption of the graphene modulator is mainly due to the partial overlap of the TE waveguide mode with the region of charge accumulation (7 nm thick alumina layer bound by the graphene layers) that is thinner than the mode size. In practice the charged region is 7 nm thick, whereas in standard charge-depletion Si modulators the active part is the entire section of the waveguide. To further reduce power consumption, it suffices to reduce the microring radius. Power consumption scales with the square of the radius. For smaller radii it is, however, necessary to choose Si microrings rather than SiN, because the index contrast is higher. For instance, in a 4 μm Si microring, power consumption would be of the order of 40 fJ/bit. However, pure phase modulation can be achieved only if the microring loss is small. If loss, for instance, due to bending losses, appears, pure phase modulation becomes a hybrid of phase and amplitude modulation. An example of an ultralow-consumption graphene-based microring modulator is reported in Ref. [18].

It must be noted that the index change in our graphene structure is based on capacitive effect, as in SISCAP modulators, whereas in plasma-dispersion Si modulators this requires current injection and therefore energy consumption. Consider that due to fabrication errors, microrings always require a trimming to lock to the operating wavelength. In a standard Si microring the best thermal trimming reported is >0.5 mW/nm, and assuming that fabrication errors on ring waveguides leads to a typical correction/trimming of the order of 1 nm, the total power consumption of carrier depletion modulators is the sum of the modulator RF consumption and trimming contributions. The trimming contribution alone is of the order of ≃0.5 mW, which is similar to the consumption of the graphene modulation by itself. Conversely, in graphene-based microring modulators, trimming is capacitive and is provided by simply applying a bias voltage. In this case there is no extra contribution to the total modulator consumption.

5. CONCLUSIONS

In conclusion, we have shown that layers of graphene embedded in the core of a SiN waveguide can be exploited to induce a change of the TE-mode propagation constant. The index change occurs when a suitable bias induces carriers in the graphene conduction band with the condition that $|\mu_C| > \hbar\omega/2$. Under this regime, graphene becomes transparent, and a tuning of the bias voltage (i.e., a change of the carrier concentration in the graphene layer) provides a large change in the real part of the dielectric constant. Phase modulation of TE modes in straight waveguides and in microring resonators has been shown. Their application in several optoelectronic functionalities as modulators, tunable filters, switches, etc., could benefit either from the efficiency of the effect or from the negligible value of insertion loss achievable. In addition, the surface charge induced in graphene is obtained by charging a capacitor, and as a consequence the induced changes do not require current flow, with benefits in terms of power consumption.

REFERENCES

1. A. K. Geim and K. S. Novoselov, "The rise of graphene," Nat. Mater. **6**, 183–191 (2007).
2. G. T. Reed, *Silicon Photonics* (Wiley, 2008).
3. J. Liu, M. Beals, A. Pomerene, S. Bernardis, R. Sun, J. Cheng, L. C. Kimerling, and J. Michels, "Waveguide-integrated, ultralow-energy GeSi electro-absorption modulators," Nat. Photonics **2**, 433–437 (2008).
4. G. T. Reed, G. Mashanovich, F. Y. Gardes, and D. J. Thomson, "Silicon optical modulators," Nat. Photonics **4**, 518–526 (2010).
5. M. Liu, X. Yin, E. Ulin-Avila, B. Geng, T. Zentgraf, L. Ju, F. Wang, and X. Zhang, "A graphene-based broadband optical modulator," Nature **474**, 64–67 (2011).
6. C. Xu, Y. Jin, L. Yang, J. Yang, and X. Jiang, "Characteristics of electro-refractive modulating based on graphene

oxide silicon waveguide," Opt. Express **20**, 22398–22405 (2012).
7. L. Yang, T. Hu, R. Hao, C. Qiu, C. Xu, H. Yu, Y. Xu, X. Jiang, Y. Li, and J. Yang, "Low-chirp high-extinction-ratio modulator based on graphene silicon waveguide," Opt. Lett. **38**, 2512–2515 (2013).
8. B. Milivojevic, C. Raabe, A. Shastri, M. Webster, P. Metz, S. Sunder, B. Chattin, S. Wiese, B. Dama, and K. Shastri, "112 Gb/s DP-QPSK transmission over 2427 km SSMF using small size silicon photonics IQ modulator and low power CMOS driver," in *Optical Fiber Conference* (Optical Society of America, 2013), paper OTh1D.1.
9. X. Xiao, H. Xu, X. Li, Z. Tao Chu, J. Yu, and Y. Yu, "High-speed, low-loss silicon Mach-Zehnder modulators with doping optimization with doping optimization," Opt. Express **21**, 4116–4125 (2013).
10. L. A. Falkovsky and S. S. Pershoguba, "Optical far-infrared properties of a graphene monolayer and multilayer," Phys. Rev. B **76**, 153410 (2007).
11. L. A. Falkovski, "Optical properties of graphene," J. Phys.: Conf. Ser. **129**, 012004 (2008).
12. G. W. Hanson, "Dyadic Green's function and guided surface waves for a surface conductivity model of graphene," J. Appl. Phys. **103**, 064302 (2008).
13. T. Stauber, N. M. R. Peres, and A. K. Geim, "Optical conductivity of graphene in the visible region of the spectrum," Phys. Rev. B **78**, 085432 (2008).
14. M. Liu, X. Yin, and X. Zhang, "Double-layer graphene optical modulator," Nano Lett. **12**, 1482–1485 (2012).
15. H. Kogelnik, "Theory of dielectric waveguide," in *Integrated Optics*, T. Tamir, ed. (Springer-Verlag, 1985), Chap. 2.
16. A. Yariv, "Critical coupling and its control in optical waveguide–ring resonator systems," IEEE Photon. Technol. Lett. **14**, 483–485 (2002).
17. L. Zhang, J.-Y. Yang, M. Song, Y. Li, B. Zhang, R. G. Beausoleil, and A. E. Willner, "Microring-based modulation and demodulation of DPSK signal," Opt. Express **15**, 11564–11569 (2007).
18. M. Midrio, S. Boscolo, M. Moresco, M. Romagnoli, C. De Angelis, A. Locatelli, and A. D. Capobianco, "Graphene-assisted critically-coupled optical ring modulator," Opt. Express **20**, 23144–23155 (2012).